NATIONAL AERONAUTICS AND SPACE ADMINISTRATION

Technical Report 32-1594

Interplanetary Navigation Using Pulsating Radio Sources

G. S. Downs

JET PROPULSION LABORATORY
CALIFORNIA INSTITUTE OF TECHNOLOGY
PASADENA, CALIFORNIA

October 1, 1974

NATIONAL AERONAUTICS AND SPACE ADMINISTRATION

Technical Report 32-1594

Interplanetary Navigation Using Pulsating Radio Sources

G. S. Downs

JET PROPULSION LABORATORY
CALIFORNIA INSTITUTE OF TECHNOLOGY
PASADENA, CALIFORNIA

October 1, 1974

Prepared Under Contract No. NAS 7-100
National Aeronautics and Space Administration

Preface

The work described in this report was performed by the Telecommunications Division of the Jet Propulsion Laboratory.

Contents

I. Introduction 1

II. A Definition of the Navigation Problem 2

A. Measurement of Position 2

B. Measurement of Time-of-Arrival 2

C. Errors in Position 3

III. Properties of Pulsar Signals 4

A. Pulse Period and Pulsar Location 4

B. Radio Spectra 4

C. Pulse Shapes 5

D. Polarization 5

E. Background Radiation 5

F. Dispersion 6

G. Scintillation 6

IV. The Evaluation of Two Schemes 6

A. Introduction 6

B. The Dispersionless Receiver 7

C. The Dispersion-Correcting Receiver 8

V. Concluding Remarks 10

References 13

Tables

1. Models of the spectra of the strongest pulsars 9

2. Navigation errors for the dispersionless receiver at 150 MHz, with 24 h of integration 10

3. Navigation errors for the dispersion-correcting receiver at F_0 = 200 and 250 MHz, ΔF = 200 MHz, with 24 h of integration 11

4. Navigation errors for F_0 = 200 MHz, ΔF = 200 MHz, and G = 10, with 24 h of integration 11

Figures

1. Barycentric coordinate system B containing the pulsar P_n and the spacecraft S_j 2
2. Representation of the measurement of time of arrival 3
3. Average pulse energy versus observing frequency: (a) Pulsar PSR 1133 + 16, (b) PSR 0329 + 54 . 5
4. Some examples of pulse intensity versus time . 5
5. Distortion due to dispersion in the interstellar medium . 6
6. The dispersionless receiver 8
7. The dispersion-correcting receiver 10

Abstract

Radio beacons with distinguishing signatures exist in nature as pulsating radio sources (pulsars). These objects radiate well determined pulse trains over hundreds of megahertz of bandwidth at radio frequencies. Since they are at known positions, they can also be used as navigation beacons in interplanetary space. Pulsar signals are weak and dispersive when viewed from earth. If an omnidirectional antenna is connected to a wideband receiver (200 MHz bandwidth centered at 200 MHz) in which dispersion effects are removed, nominal spacecraft position errors of 1500 km can be obtained after 24 h of signal integration. An antenna gain of 10 dB would produce errors as low as 150 km. Since the spacecraft position is determined from the measurement of the phase of a periodic signal, ambiguities occur in the position measurement. Simultaneous use of current spacecraft navigation schemes eliminates these ambiguities.

Interplanetary Navigation Using Pulsating Radio Sources

I. Introduction

A scientific mission to the outer planets will result in an improved ephemeris of these planets. Subsequent missions would then become easier, hence cheaper, because less maneuvering would be required. Imagine a spacecraft located in a spherical coordinate system centered at the sun. The range of a particular spacecraft can be measured with uncertainties as low as 5 m. Angular positions of the spacecraft are relatively larger and increase with increasing range. For example, an error of 0.1 arc-s in angular position is an error of 300 km at the distance of Jupiter and 2300 km at the distance of Pluto. These errors are small when compared to the ephemeris uncertainties. In late 1973, these uncertainties were 800 km for Jupiter and 90,000 km for Pluto. It is then clear that a flyby of a spacecraft will lead to better ephemerides. This report discusses the use of naturally occurring pulsating radio sources to fix a spacecraft's position within a given coordinate system.

One is reminded of the Loran-C navigation scheme, in which the navigator can locate his position on the surface of the earth by obtaining relative time delays between a master radio transmitter and one or more of its slave transmitters. He then locates himself at the intersection of two circles. A similar system could be used for interplanetary navigation by placing radio transmitters on or near selected planetary surfaces.

A natural navigation system is available to us in the form of pulsating radio sources (pulsars). When pulsars were first discovered, the possibility that they were the beacons of an intragalactic navigation scheme was considered. (This was known as the LGM hypothesis, where LGM = little green men.) This hypothesis was soon abandoned when it was found that pulsars radiate over many hundreds of megahertz. In this discussion, we turn this hypothesis around and ask how we might use such objects. As in the case of the Loran-C transmitters, these sources are at known locations, and they emit pulses of radiation a few milliseconds wide at regular intervals (typically 0.5 s) and at predictable times. They are within our galaxy but outside the solar system. They are therefore beyond our control, but have useful lifetimes of several million years. They are intrinsically powerful emitters, averaging 10^{17} J in each pulse between 100 and 10,000 MHz (that is, the output of Hoover Dam for 3 years). However, the distances to these sources are so large (up to 10^{22} m) that energy densities in the wavefronts are often attenuated more than 450 dB. Radiometers on or near earth will then detect pulses with only 10^{-24} J/m^2 of

antenna area, suggesting that long integration times will be needed to obtain usable signal-to-noise ratios.

The measurement problem is defined in Section II in only enough detail to allow a calculation of expected errors in the spacecraft position. In Section III, we consider the appropriate properties of pulsars and their surroundings. An analysis of a navigation system using pulsars as the beacons is presented in Section IV, and concluding remarks are made in Section V.

II. A Definition of the Navigation Problem

The position of the spacecraft in a particular coordinate system is calculated by comparing the arrival time of a particular pulse at the spacecraft with the arrival time of that pulse at the origin. Alternatively, we measure the phase of the pulse train at the spacecraft relative to a given epoch and compare it with a similar measurement at the origin of the coordinate system. The measurement process involves errors because of noise fluctuations from the receiver, the background radiation from the galaxy, and the pulsar itself. The size and orientation of the ellipsoid describing the uncertainty in the spacecraft position can be estimated if enough system parameters are known.

A. Measurement of Position

Consider a pulsar located in the direction given by unit vector $\mathbf{U}_p$ and a spacecraft whose position is defined by a vector S (Fig. 1). The difference in the time-of-arrival (TOA) of a pulse or wavefront at the spacecraft and at origin B is

$$T = \frac{1}{c}\mathbf{S} \cdot \mathbf{U}_p \tag{1}$$

where c is the velocity of propagation, T is the quantity measured, and the components S_x, S_y, and S_z of S are the unknowns. A minimum of three independent equations are needed, so at least three pulsars must be included in Eq. (1). We therefore make the following measurements:

$$T_i = \frac{1}{c}[S_x \cos(\delta_i)\cos(\alpha_i) + S_y \cos(\delta_i)\sin(\alpha_i) + S_z \sin(\delta_i)] \tag{2}$$

where the subscript refers to a particular pulsar and takes on values of 1, 2, and 3. The angular coordinates α_i and δ_i are the right ascension and declination, respectively, of the ith pulsar. Equation (2) can be written in matrix form as

$$(T) = \frac{1}{c}(A)(S) \tag{3}$$

where (T) and (S) are 3×1 matrices and (A) is a 3×2 matrix. We then solve for (S) if the inverse (A^{-1}) of (A) exists:

$$\begin{pmatrix} S_x \\ S_y \\ S_z \end{pmatrix} = (S) = c(A^{-1})(T) \tag{4}$$

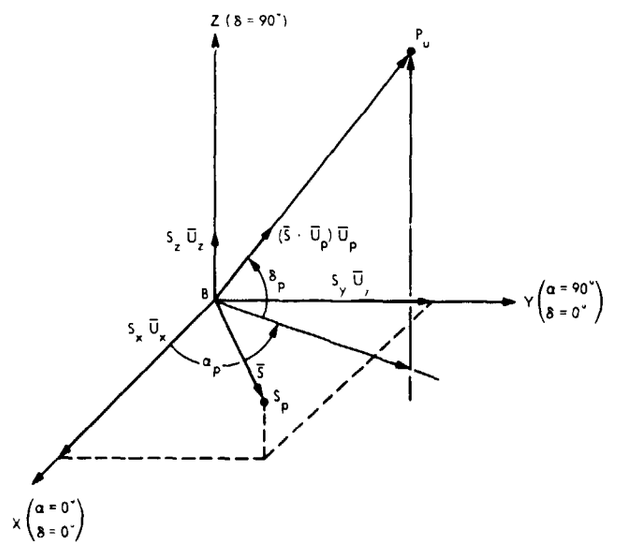

Fig. 1 Barycentric coordinate system B containing the pulsar P_u and the spacecraft S_p. The objective is to measure the components of the spacecraft vector $\bar{S}$

B. Measurement of Time-of-Arrival

The errors associated with the measurements described by Eq. (4) depend on how the measurements are made. The measurement procedure is represented in Fig. 2. In this analysis, we assume that the signal, band-limited with a rectangular passband, is square-law detected so that the receiver output is proportional to the average power. The detected signal is then passed through a low-pass filter to reduce noise fluctuations. The filtered signal is filtered further by correlating the output with a noise-free template representing the average shape of the received pulse. That is, the signal is passed through a matched filter to maximize the signal-to-noise ratio (S/N). It is assumed that the average pulse shape or template has been obtained in a separate observing program. It is the result of adding several thousand pulses together and is

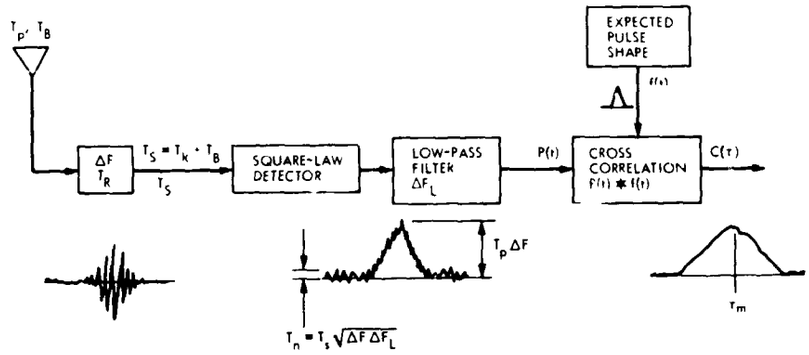

Fig. 2 Representation of the measurement of time-of-arrival. The error in the measurement is due to noise proportional to T_S (receiver noise T_R and sky noise T_B) within bandwidth ΔF

represented by $f(t)$ in Fig. 2. The correlation process is performed such that the time delay τ between the template and the signal is measured relative to a particular epoch t_0. The maximum value of the correlation function $c(\tau)$ occurs at delay τ_m. The delay τ_m is the TOA of the pulse or the phase of the pulse train relative to t_0.

Random fluctuations in the detected signal cause random fluctuations in $c(\tau)$, so there is an uncertainty associated with the measurement of τ_m. The rectangular RF filter has a bandwidth of ΔF. Consider the integrator following the square-law detector to be a rectangular low-pass filter with a bandwidth of ΔF_L. The dc output of the detector is proportional to $T_p \Delta F$, where T_p is the antenna temperature of the pulsar. The fluctuating component of the detector output has an autocorrelation function $R_n(t)$. Represent the pulse template by $f(t)$, where the maximum value is 1.0. It can then be shown that the variance of a TOA measurement is (Ref. 1)

$$\sigma_{\tau_m}^2 \cong \frac{2T_s^2 \Delta F_L}{T_p^2 \Delta F} \frac{\Delta t}{\int \dot{f}^2 dt} \tag{5}$$

where T_s is the equivalent noise temperature of the system. We have defined an integration time $\Delta t = 1/2\Delta F_L$. (See Ref. 2 for a discussion of integration times.) Equation (5) is valid if σ_{τ_m} is less than the pulse width.

It seems reasonable that we can define time more accurately with a strong, narrow pulse than with a weak, broad pulse. These facts are demonstrated in the two factors of Eq. (5).

C. Errors in Position

Three particular pulsars are included in the navigation scheme. If a large number of measurements were performed of each T_i represented in Eq. (3), the errors would be independent and distributed normally about some true value $\langle T_i \rangle$. The covariance matrix of the series of measurements is then diagonal and written as

$$\Lambda = \begin{bmatrix} \sigma_1^2 & 0 & 0 \\ 0 & \sigma_2^2 & 0 \\ 0 & 0 & \sigma_3^2 \end{bmatrix} \tag{6}$$

where the subscript on $\sigma_{\tau_m}^2$ has been simplified. The joint probability density function of the deviations from T_i is then the normal distribution

$$p(t_1, t_2, t_3) = \frac{1}{(2\pi)^{3/2}|\Lambda|^{1/2}} \exp\left[-\frac{1}{2}\sum_n \sum_m (\Lambda^{-1})_{nm} t_n t_m\right] \tag{7}$$

where $t_n = T_n - \langle T_n \rangle$.

The errors in spacecraft location can be found from the coordinate transformation of Eq. (4). The spacecraft positions S_x, S_y, and S_z will be normally distributed about true mean values S_{x0}, S_{y0}, and S_{z0}. The random deviations $r_1 = S_x - S_{x0}$, etc., will have a covariance matrix (μ) given by

$$(\mu) = (A^{-1})(\Lambda)(A^{-1})^T \tag{8}$$

(T denotes transposition of rows and columns). The probability density function of the errors is then

$$p(r_1, r_2, r_3) = \frac{1}{(2\pi)^{3/2}|\mu|^{1/2}} \exp\left[-\frac{1}{2}\sum_n \sum_m (\mu^{-1})_{nm} r_n r_m\right] \tag{9}$$

where $n, m = 1, 2, 3$ and $(\mu^{-1})_{nm}$ denotes a particular element of the symmetric inverse matrix (μ^{-1}).

The summation in Eq. (9) is a quadric form $F_q = (R)^T(\mu^{-1})(R)$, where (R) is the column matrix of errors r_1,

r_2, and r_3. The form F_q is positive definite, so a particular value of F_q defines an ellipsoid of a certain size centered at the location calculated in Eq. (7). Also, the particular value of F_q determines the probability that the spacecraft is actually located within the ellipsoid. For example, when $F_q = 4$ the probability that the vector S_0 lies within the ellipsoid centered on S is 0.95. It is then desirable to view the error ellipsoid in a coordinate system aligned with its principal axes. This is equivalent to diagonalizing the matrix (μ^{-1}). If the new inverse covariance matrix is $(\mu^{-1})'$, then we need a coordinate transformation (Q), usually a series of rotations, such that

$$(\mu^{-1})' = (Q)^T(\mu^{-1})(Q)$$

If the columns of (Q) are made up of the components of the eigenvectors of (μ^{-1}), then (Q) will have the desired properties (see, for example, Ref. 3).

Let λ_1, λ_2, and λ_3 represent the eigenvalues of (μ^{-1}) and $\mathbf{e}_n = (e_{n1}, e_{n2}, e_{n3})$ represent the eigenvector associated with λ_n. The components of $\mathbf{e}_n$ are projections of $\mathbf{e}_n$ onto the original reference frame defined in Fig. 1. The eigenvalues are found from finding the three roots of

$$|(\mu^{-1}) - \lambda(I)| = 0 \qquad (10)$$

where (I) is the identity matrix. The eigenvectors can be found by noting that, letting $(\rho) = (\mu^{-1})$ to simplify notation,

$$(\rho_{11} - \lambda_1)e_{11} + \rho_{12}e_{12} + \rho_{13}e_{13} = 0 \qquad (11a)$$

$$\rho_{21}e_{21} + (\rho_{22} - \lambda_2)e_{22} + \rho_{23}e_{23} = 0 \qquad (11b)$$

$$\rho_{31}e_{31} + \rho_{32}e_{32} + (\rho_{33} - \lambda_3)e_{33} = 0 \qquad (11c)$$

Equations (11a–c) can be viewed as the expansion of the determinant $|(\rho) - \lambda_n(I)|$, which must equal zero. Therefore, the vector components e_{nm} can be the cofactors of the elements in the nth row of the matrix $(\rho) - \lambda_n(I)$. Normalizing the vector $\mathbf{e}_n$ such that

$$\sum_{m=1}^{3} e_{nm}^2 = 1$$

produces a unit vector aligned along the principal axis associated with the half-size λ_n.

III. Properties of Pulsar Signals

Several important phenomena and facts observed in or about electromagnetic waves from pulsars are presented and discussed here. Only the properties which will affect a navigation attempt are discussed.

A. Pulse Period and Pulsar Location

The interval between the pulses (pulse period) and the angular position of the pulsar are the most difficult parameters to determine. The period increases slowly with time and, in general, the pulsar moves in the sky (proper motion). These two parameters are discussed together because they are measured simultaneously. Their effect on the times of arrival of the pulses at a chosen observing point can be easily noted if the signal is sufficiently strong. An error in position of 1 arc-s will produce an arrival-time error on earth of 2.5 ms, ordinarily an easily detected error. Also, apparently small errors in period can multiply over a large time extent so that predicted arrival times are seriously in error. For example, consider a pulsar in which the period $P = 1$ s and the uncertainty in the period is given by $\Delta P/P \sim 1 \times 10^{-6}$. A prediction of an arrival time 1 week later may well be required in this navigation scheme. In this case, the prediction will differ from reality by 600 ms.

Since period and position do affect the results of time-of-arrival measurements, they are solved for simultaneously. Note that pulsar position affects earth-bound measurements because the earth is in motion. The analysis of the results of a series of TOA arrival measurements requires an ephemeris of the earth in a coordinate system whose origin is the center of mass (barycenter) of the solar system. Therefore, although pulsar positions can be determined to an accuracy of 0.01 arc-s, these errors apply only within the reference frame defined by the ephemeris. Several observing programs have been or are being carried out to determine period, position, and slow changes in time of both quantities. The most accurate observing program known to this author is carried out at the Jet Propulsion Laboratory. This observing program is described theoretically in Refs. 4 and 5, and some results are presented in Ref. 6.

B. Radio Spectra

The peak flux density B_p (measured in W/m²/Hz) of a pulse changes with observing frequency. One generally sees a decreasing pulse strength with increasing frequency. A common measure of the spectrum of a pulsar is the energy contained within a pulse

$$E(F) = B_p(F)\int f(t)dt$$

This quantity varies from pulse to pulse (see section H), but a particular value is obtained after averaging over

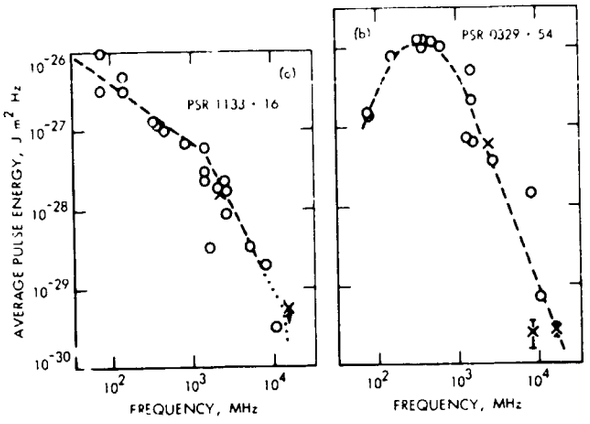

Fig. 3 Average pulse energy versus observing frequency: (a) Pulsar PSR 1133 + 16, (b) FSR 0329 + 54

many pulses. Of course, this average energy changes with frequency, and two examples of $E(F)$ are presented in Fig. 3. The behavior in Fig. 3a is typical, but exceptions do occur (Fig. 3b).

C. Pulse Shapes

Imagine a simple receiver in which an RF signal is square-law detected, then low-pass filtered to minimize noise fluctuations. The output of this receiver is proportional to the average RF energy at a given time, averaged over a time determined by the low-pass filter. Outputs of such a receiver are shown in Fig. 4 for several pulsars. This particular sequence of pulse shapes was chosen to illustrate the variety of shapes among pulsars. One should also note the differences in pulse width, or sharpness, and the different peak S/N ratios.

D. Polarization

The emissions of pulsars are generally randomly polarized, obtaining some linear polarization in some cases. A good discussion of this property of several pulsars is given in Ref. 7. If one were forced to use a receiving antenna sensitive to one polarization only, it should be a circular polarization. The polarization may be linear or circular if both orthogonal modes are received.

E. Background Radiation

Outside the earth's atmosphere, synchrotron radiation from the galaxy contributes the most radiation to the general (and unwanted) system noise. This contribution T_B to the equivalent noise temperature T_S of the receiver system varies with position in the sky. At 200 MHz, the

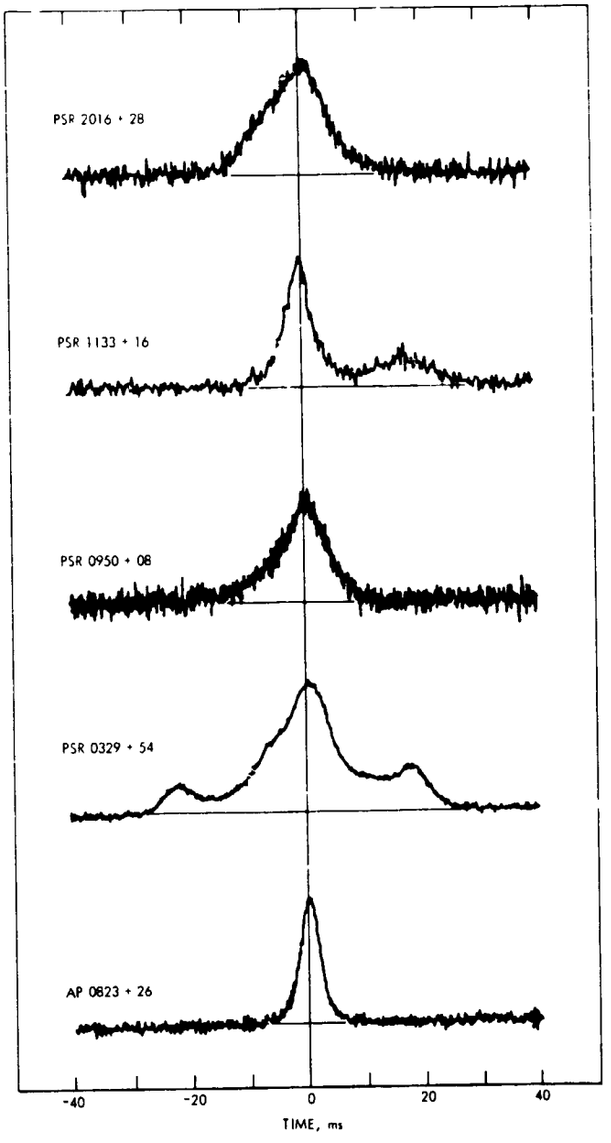

Fig. 4 Some examples of pulse intensity versus time

galactic center is at a temperature of 1200 K, while the galactic poles are near 130 K. Antennas used in this navigation system will be of low enough gain that the average temperature T_B will suffice. The average temperature varies with frequency, dropping from 1350 K at 100 MHz to 25 K at 500 MHz. Using data presented in Ref. 8, the system temperature can be represented as

$$T_S = T_R + T_B$$

or

$$T_s = T_R + 3.0 + 215\left(\frac{200}{F}\right)^{2.4} \text{ K} \qquad (12)$$

where T_R is the equivalent noise temperature of the first receiver amplifier and F is the observing frequency in megahertz.

F. Dispersion

The index of refraction in an ionized medium changes with frequency. The interstellar medium consists predominantly of ionized hydrogen with densities low enough that collisions are not important. In this case, the group velocity of the pulse of energy is

$$\frac{v}{c} \approx 1 - \frac{1}{2}\frac{F_N^2}{F^2}$$

if $F^2 \gg F_N^2$, c is the free-space velocity, and $F_N^2 \approx 8.1 \times 10^7 N_e$, where F_N is in hertz and N_e the electron density, is in electrons per cubic centimeter. In traveling a distance L (measured in parsecs, where 1 parsec = 3.08×10^{13} km), a time delay of ΔT s relative to the free-space propagation time is introduced:

$$\Delta T = \frac{4.1 \times 10^{15}}{F^2}\int_0^L N_e dl$$

This time delay changes with frequency, and for small changes in frequency, we find that

$$\dot{F} = \frac{dF}{dt} = -\frac{1.21 \times 10^{-9} F^3}{\int_0^L N_e dl} \text{ MHz/s} \qquad (13)$$

where F is now in megahertz; $\int N_e dl$ is the number of electrons in a column 1 cm^2 in cross-section and L parsec long and is referred to as the dispersion measure.

A dispersed signal will then sweep through a receiver passband, as illustrated in Fig. 5. The instantaneous bandwidth of the dispersed pulse will then be less than for the original undispersed pulse, and distortion is the result. Increased dispersion produces not only increased delay and distortion but also lower peak S/N ratios. Therefore, a wider bandwidth does not necessarily mean the increased S/N ratio usually obtained in radiometry. Dispersion is the phenomenon which most seriously affects the signal; this phenomenon is dealt with directly in Section IV.

G. Scintillation

The shape and amplitude of individual pulses of radiation differ significantly from pulse to pulse for a particular pulsar (see e.g., Ref. 9). However, when one averages over several hundred pulses, these variations in shape and amplitude approach stable shapes and values. Inhomogeneities in the interstellar plasma, acting as large moving lenses, impose variations of several minutes on the pulse amplitude (see, e.g., Ref. 10). These variations wash out after several hours of averaging, and are not considered a deleterious effect in this study.

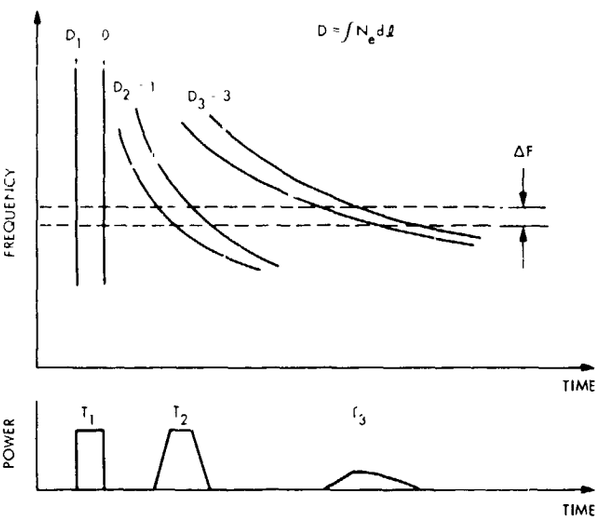

Fig. 5 Distortion due to dispersion in the interstellar medium

IV. The Evaluation of Two Schemes

A. Introduction

The present objective is to choose a set of three pulsars which yields the lowest navigation errors. The pulsar period and spectrum must be known. Then, for a particular system temperature T_s, a peak antenna temperature T_p of the pulsar, and a post-detection integration time Δt, one can superimpose N pulses and obtain the first term of Eq. (5). Throughout this analysis, it was assumed that the antenna gain $G = 1$ and that the antenna is sensitive to only one polarization. The receiver is a direct radiometer, as described in Fig. 2, with the correlation taking place on earth. With these assumptions, T_p can be expressed at a particular frequency as

$$T_p(F) = \frac{B_p(F)A_e}{2k}$$

where k is Boltzmann's constant, A_e is the effective area of the antenna, and $B_p(F)$ is the peak flux density of the pulse. Since $G = 4\pi F^2 A_e/c^2$,

$$T_p F = B_p F \frac{c^2}{8k\pi} \frac{G}{F^2} \tag{14}$$

The system temperature T_s is calculated using $T_R = 300$ K in Eq. (12). It is assumed that $T_s \gg T_p$. Substitution of Eq. (14) into Eq. (5), taking into account the superposition of N pulses, yields

$$\sigma_{\tau_m}^2 = \frac{2T_s^2 \Delta F_I}{N \Delta F} \left(\frac{8k\pi F^2}{B_p c^2 G}\right)^2 \frac{\Delta t}{\Sigma (\Delta f / \Delta t')^2 \Delta t'} \tag{15}$$

where the integral in Eq. (5) has been written in discrete form since the templates are available only in discrete form. The sampling interval is $\Delta t'$.

At first glance, it would seem desirable to make ΔF and ΔF_I as large as possible. When the time it takes the dispersed signal to sweep through the passband becomes as large as the pulse width, the sharp structure in the pulse is lost. Unless dispersion effects are taken out, an unlimited RF bandwidth will result in poorer time resolution. Furthermore, close scrutiny of Eq. (15) shows that the expression is, except for the effects of smoothing, independent of ΔF_I. Apparently, the noise contribution appears not so much as a S/N ratio but as the amount of noise energy in the time interval needed for a significant decorrelation of the noise. This time is Δt in Eq. (15). The bandwidth ΔF_I does have an effect, though, on the sharpness of the pulse. Limits on ΔF and ΔF_I must then be found.

In the next two sections, navigation errors are calculated for different combinations of pulsars. In the Section B, it is assumed that the receiver cannot correct for dispersion in the RF passband, and this results in narrow bandwidths and larger position errors. In the Section C, a receiver is constructed to compensate for dispersion effects, so smaller errors are obtained by using larger bandwidths. Errors peculiar to each pulsar were calculated using Eq. (5). Position errors obtained using a given set of three pulsars were determined as described in Section IIC.

B. The Dispersionless Receiver

The simplest spacecraft receiver possible is considered first to provide insight into the navigation problem. The receiver is represented in Fig. 6. The antenna configuration remains unspecified, but it is assumed to cover the celestial sphere, each pulsar experiencing an antenna gain of unity. Three different receiver channels are needed since the spectra and dispersion measures differ among pulsars. Integration or superposition of the pulses over a long time interval (hours) will be necessary, so the output of each receiver channel is fed into its own digital sampling and storage device. Sampling and the storage address are coordinated and controlled by a controlled oscillator. Since the spacecraft is in motion, significant doppler shifts will be experienced. Failure to adjust the sampling rate so that the same number of samples are taken during each pulse period will result in severe smearing of the pulse. Therefore doppler shift information is sent to the spacecraft on the uplink before an observing session is to begin. The resulting integration is sent to earth-based computers via the downlink along with the time at which sampling started. The number of pulses superimposed depends on how rapidly the expected doppler shift is changing. One could, in principle, superimpose pulses for several days if no changes were occurring. During encounters with planets, superpositioning may last only 1 h before an "update" of the controlled oscillator is necessary. Further superposition then takes place on earth. A monitor of the frequency standard driving the controlled oscillator is maintained. Slow drifts in the standard are accounted for in the information supplied to the controlled oscillator.

The performance of this system was evaluated in two stages. First, the error σ_{τ_m} was calculated at several receiver frequencies between 100 and 1650 MHz for the first 18 entries in Table 1. The last nine entries are not observable at Goldstone. The spectra of these pulsars are known through a compilation of data taken from the literature on pulsars. The compilation presented here does not appear in the literature. The spectra were approximated by power-law functions within one or more segments of the 80- to 10,000-MHz frequency range. These segments are denoted in Table 1, the last segment in each row ending at 10,000 MHz. The low-frequency limit F_L and the appropriate exponent α are listed for each segment. In segment 1, the average pulse energy is given by $J_c(F_H/F)^\alpha$, where F_H is the highest frequency in segment 1 (300 MHz in the case of pulsar 0628, e.g.), and J_c is the energy at F_H. In segments 2 and 3, the energy is given by $J_c(F_L/F)^\alpha$. Although more than eighty pulsars are known, only the strongest are considered here.

System noise temperatures were calculated from Eq. (12). The integrals $\int(\dot{f})^2 dt$ were calculated from templates measured at 2388 MHz in a JPL research program on the first 18 pulsars in Table 1. Although the templates $f(t)$ are slow functions of frequency, it was assumed that they do not vary significantly with frequency because of a lack of information at lower frequencies. The RF bandwidth ΔF was slowly widened until $f(t)$ was significantly smoothed. The appropriate smoothing time was calculated using the dispersion measures peculiar to a given pulsar. Also, the

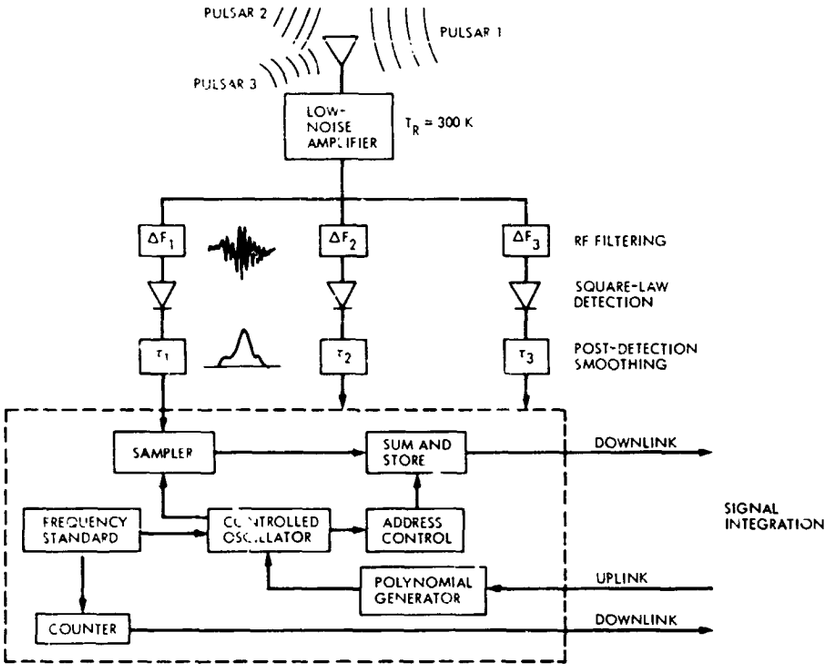

Fig. 6 The dispersionless receiver

post-detection bandwidth was slowly decreased until $f(t)$ was affected. In this way, limits on ΔF and ΔF_i were placed on each receiver channel for several possible operating frequencies. It was assumed that pulses were superimposed for 24 h. This completed the first stage.

The pulsars were brought together three at a time in the second stage of the analysis. The positions used are readily found in the literature. Eigenvalues of the inverse covariance matrix μ^{-1} were calculated for the case $F_q = 4$, corresponding to solving for the 95%-confidence ellipsoid (see the discussion of Eq. 9). A total of 816 combinations were analyzed. The results were considered in order of increasing ellipsoid volume. The lowest errors obtainable with this system are presented in Table 2 along with the three pulsars used to obtain the spacecraft position. Limiting values of ΔF and ΔF_i are presented with expected arrival-time errors and S/N ratios. The size of each principal axis is compared to the diameter D_J of Jupiter (1.5×10^5 km).

The inadequacy of this scheme is readily apparent in Table 2, since the conditions for the validity of Eq. (5) are not met. The values of σ_r are greater than the pulse width in each case. This is also exhibited by S/N ratios less than 1.0. A more promising scheme is analyzed in Section C.

C. The Dispersion-Correcting Receiver

A large limitation in the previous scheme is the confinement to narrow bandwidths. It was therefore postulated that a dispersive filter can be built for a spacecraft which will compensate for the interstellar dispersion. Such a system is represented in Fig. 7. The dispersive filter is conceptually represented as a parallel set of filters of width ΔF_i followed by delay T_i. (Note that $\Delta \mathcal{F} = \Sigma \Delta F_i$.) The progression of delays depends on the dispersion measure of the particular pulsar. The rest of the receiver is identical to that previously described.

The last nine pulsars in Table 1 were included in the analysis. It was hoped that inclusion of these southernmost pulsars would produce an error ellipsoid more spherical in shape than that presented in Table 2. Little is known about the spectrum and pulse shape of these particular objects. The spectra were therefore conservatively modeled about published average strengths at 400 MHz. Below 400 MHz, the spectra were assumed to be flat ($\alpha = 0.0$), which means that the peak flux density at 100 MHz may have been underestimated by as much as 10. The detailed pulse shapes are practically unknown, so templates for pulsars of approximately the same period and overall pulse width were assigned to these less-studied pulsars.

Table 1. Models of the spectra of the strongest pulsars

Entry	Pulsar	J_ν, J/m²/Hz	1		2		3	
			F_L, MHz	α	F_L, MHz	α	F_L, MHz	α
1	0031	7.0×10^{-27}	80	1.9				
2	0329	1.0×10^{-26}	100	−1.3	360	0.0	800	2.75
3	0525	1.0×10^{-26}	100	1.8				
4	0628	1.0×10^{-26}	80	0.0	300	1.9		
5	0823	1.0×10^{-27}	80	0.0	500	1.85		
6	0950	4.0×10^{-28}	80	1.0	1000	2.5		
7	1133	6.0×10^{-28}	100	0.8	1400	2.1		
8	1237	1.0×10^{-27}	100	0.0	300	1.3		
9	1642	1.0×10^{-26}	80	0.0	150	2.2		
10	1706	5.0×10^{-28}	80	0.0	1000	2.0		
11	1749	6.0×10^{-27}	80	0.0	500	2.85		
12	1818	1.0×10^{-27}	80	0.0	400	2.6		
13	1911	2.0×10^{-27}	80	0.0	300	2.5		
14	1929	4.0×10^{-28}	100	0.0	1000	1.9		
15	1933	4.0×10^{-28}	100	0.0	1000	3.1		
16	2021	1.0×10^{-27}	100	0.0	1000	1.6		
17	2045	8.0×10^{-28}	100	0.0	1000	2.6		
18	2218	1.0×10^{-26}	100	2.2				
19	0254	5.0×10^{-27}	100	0.0	400	2.0		
20	0940	1.0×10^{-27}	100	0.0	400	2.0		
21	0959	1.0×10^{-27}	100	0.0	400	2.0		
22	1359	5.0×10^{-28}	100	0.0	400	2.0		
23	1426	1.0×10^{-27}	100	0.0	400	2.0		
24	1451	2.0×10^{-27}	100	0.0	00	1.8		
25	1530	1.0×10^{-27}	100	0.0	400	2.0		
26	1727	1.5×10^{-27}	100	1.0	400	2.0		
27	1747	1.0×10^{-27}	100	1.7	400	2.0		

The bandwidth ΔF was fixed at 200 MHz and centered about F_0 = 200 MHz. Arrival-time errors were calculated for 27 pulsars. A range of post-detection bandwidths were considered for the purpose of finding limits on ΔF_L. No dispersion smearing was considered since the dispersion-correcting filter eliminates this effect. The pulsars were then analyzed in groups of three (2925 combinations) to determine navigation errors. The results were ranked according to increasing volume of the ellipsoid. The three best combinations are presented in Table 3.

The analysis was repeated with a center frequency of 250 MHz to determine the sensitivity of the errors to operating frequency. The results, also presented in Table 3, show that a center frequency of 200 MHz is better than

Table 2. Navigation errors for the dispersionless receiver at 150 MHz, with 24 h of integration

Pulsar	ΔF, Hz	ΔF_L, Hz	σ_τ, ms	S/N ratio
0950	9.0×10^5	300	41	0.11
1642	5.6×10^4	380	25	0.12
1749	5.7×10^4	280	66	0.06

250 MHz and imply that a slightly narrower bandwidth may be better.

The results presented in Table 3 indicate that with this low-cost navigation scheme, one can navigate among the outer planets with an accuracy comparable to the present navigation scheme. The system has the following characteristics:

(1) Each pulsar is viewed with an antenna gain of 1.0.

(2) The antenna is sensitive to one polarization.

(3) The receiver is a direct radiometer.

(4) Dispersion effects in the receiver passband are eliminated.

(5) The average pulse shapes are known, the detection process is square-law, and the time-of-arrival is determined by correlating the detected signal with the average template.

Several alterations that will improve this system are discussed in Section V.

V. Concluding Remarks

The expected navigation errors listed in Table 3 would be extremely attractive if they were smaller by a factor of 10. This decrease can be most easily obtained by increasing the antenna gain. A broadband or frequency-independent antenna is needed to cover the frequency band of 100 to 300 MHz. Imagine, then, a trapezoidal wire antenna supported by two booms. Another trapezoidal wire antenna is rotated 90 deg in space and physically combined with the other wire antenna to form a truncated-pyramid shape. The base would be 1.5 to 2.0 m on a side and the "top" or small end of the pyramid about 0.5 m. The height of the truncated pyramid would be about 0.5 m. (A 45-deg angle exists between the centerline and each side of the antenna; see Ref. 11.)

An antenna such as this would have a gain of 7 to 8 dB and a circular beam of 66-deg half-power width. Nine such antennas would be needed to cover the entire sky. This is probably not possible since such a structure of wires would interfere with the communications antennas. Also, complete sky coverage allows the sun's radiation to cause an increase in the equivalent noise temperature of the receiving system. Only three antennas are needed if

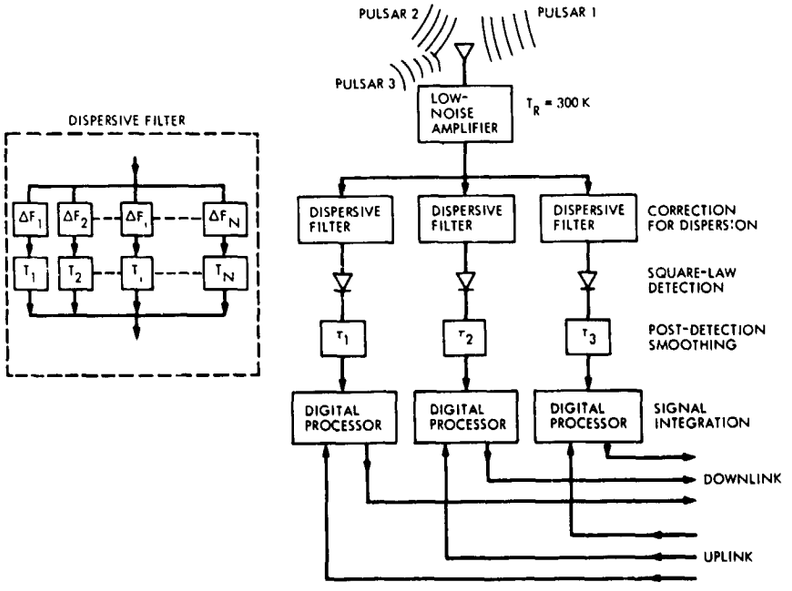

Fig. 7 The dispersion-correcting receiver

Table 3. Navigation errors for the dispersion-correcting receiver at F_0 = 200 and 250 MHz, ΔF = 200 MHz, with 24 h of integration

Combination	Pulsar	ΔF_D, Hz	σ_T, ms		Principal axis	Size, km	
			F_0 200	F_0 250		F_0 200	F_0 250
1	1642	500	0.40	0.74	1	650	1160
	1749	600	0.90	1.07	2	1800	4140
	2218	4600	0.80	2.11	3	1520	2130
2	1642	500	0.40	0.74	1	660	1230
	1911	3000	1.80	2.23	2	3800	5800
	2218	4600	0.80	2.11	3	1540	3190
3	0950	5000	1.80	3.03	1	660	1220
	1642	500	0.40	0.74	2	3820	6980
	2218	4600	0.80	2.11	3	1590	3900

the spacecraft maintains a constant orientation relative to the star.

This antenna system would be sensitive to both polarizations, so an improvement of 10 dB can be expected. Using combination 1 of Table 3, the low errors of Table 4 can be obtained.

A few remarks concerning ephemeris and timing errors are necessary. There is always some uncertainty in the position of a particular pulsar. This causes some uncertainty in referring the arrival time of a particular pulse at the earth to the origin of the coordinate system. If the position error is 0.01 arc-s, the maximum error in arrival-time is 24 μs, a barely noticeable effect. The spacecraft sees the same position error. At the distance of Pluto, the maximum error in referring an arrival time to the origin (or alternatively, in the solutions to Eq. 4) is magnified to about 0.9 ms. This is a significant systematic error.

Ephemeris errors have an effect on this scheme in that the position of earth relative to the origin of the coordinate system (usually the center-of-mass of the solar system) is in error by about 35 km in current ephemerides. This amounts to an error in arrival time of about 120 μs. Although this is a small error for the navigation system, it is not small for earth-based arrival time measurements; i.e., pulsar arrival-time data could be used to improve an ephemeris of earth.

Table 4. Navigation errors for F_0 = 200 MHz, ΔF = 200 MHz, and G = 10, with 24 h of integration

Principal axis	Size, km
1	65
2	180
3	150

The determination of the pulsar models is not very sensitive to the location of the receiving antennas. A 1-km error in station location causes a 3.3 μs error in arrival time. This error is not significant in current measurements.

Clock errors affect arrival time measurements directly. These errors should be 1/10 or less of the desired arrival time accuracy. This applies to spacecraft and earth-based clocks.

The definition of epoch appears in this navigation scheme as well as in the schemes currently in use. During 24 h of integration, a spacecraft can move as much as 10^8 km. One experiences the same conceptual problem in current systems when integrating range and doppler shift errors over 12 h of spacecraft tracking.

The acceleration of the spacecraft creates a need for second-order doppler shift corrections. If the spacecraft is accelerating uniformly, the actual phase of the pulse train drifts relative to the phase of the zero-order pulse train (constant period modified by a constant doppler shift) by an amount proportional to the square of time. Representing the velocity in the direction of the pulsar by $v_0 + v_1(t$

$- t_0)$, the phase drift, expressed as a fractional part of the rest-frame period, becomes

$$\Delta N = \frac{v_1}{2c} \frac{(t - t_0)^2}{P_0} \left(1 + \frac{v_0}{c}\right)^{-2}$$

where c is the velocity of light and v_0 is the zero-order velocity. The integrated pulse is smeared over an entire pulse period if (1) the polynomial of Fig. 6 is zero-order, (2) the integration time $t - t_0$ is 24 h, and the acceleration v_1 is only 0.08 m/s^2. Therefore, acceleration must be allowed for in the polynomial generator. It may be unreasonable to expect a uniform acceleration, so a second-order model of the velocity may be needed.

This navigation scheme does require a continuation of earth-based measurements of pulsar arrival times. Discontinuities or sudden jumps in the period of two fast pulsars have been observed (see, e.g., Ref. 12). Although no such large jumps have been observed in the pulsars included in this study, such possibilities cannot be eliminated. In addition, pulsar models of period and position need to be updated because of small errors in the models caused by errors in arrival time measurements.

Finally, it should be pointed out that there is an ambiguity in this navigation technique. The measurement of the pulse arrival time for a given pulsar relative to a given epoch is the measurement of the phase of a pulse train. There is an ambiguity of an integral number of pulse periods NP in the arrival time. In fact, we determine a series of planes separated in space by Pc km (3×10^5 km for a 1-s pulsar). In using three pulsars, we then determine a three-dimensional grid of possible spacecraft locations. Simultaneous use of current navigation techniques would eliminate these ambiguities.

References

1. Reichley, P. E., private communication.
2. Bracewell, R. N., *The Fourier Transform and Its Applications*, Chapter 16, McGraw-Hill Book Co., Inc., New York, 1965.
3. Hildebrand, F. B., *Methods of Applied Mathematics*, Prentice Hall, Englewood Cliffs, N. J., 1952.
4. Downs, G. S., "Pulsar Periods," in *The Physics of Pulsars*, A. M. Lenchek, ed., Gordon and Breach, New York, 1972.
5. Reichley, P. E., Downs, G. S., and Morris, G., *JPL Quart. Tech. Rev.*, Vol. 1, No. 2, Jet Propulsion Laboratory, Pasadena, Calif., July 1971, p. 80.
6. Reichley, P. E., Downs, G. S., and Morris, G., *Ap. J. (Lett.)*, Vol. 159, 1970, p. 35.
7. Manchester, R. N., *Ap. J. Supp. Sers. No. 199*, Vol. 23, p. 283.
8. Kraus, J., *Radio Astronomy*, McGraw-Hill Book Co., Inc., New York, 1966.
9. Ekers, R. D., and Moffet, A. T., *Nature*, Vol. 220, 1968, p. 227.
10. Downs, G. S., and Reichley, P. E., *Ap. J. (Lett.)*, Vol. 163, 1971, p. 11.
11. Rumsey, V. C., *Frequency Independent Antennas*, Chapter 5. Academic Press, New York, 1966.
12. Reichley, P. E., and Downs, G. S., *Nature*, Vol. 234, 1971, p. 48.

NASA — JPL — Coml., L.A., Calif